Electronic Supplementary Information

Convolution of chemoattractant secretion rate, source density, and receptor desensitization direct diverse migration patterns in leukocytes

Yana Wang and Darrell J. Irvine

Correspondence should be addressed to D.J.I. 77 Mass Ave, Cambridge MA 02139, Phone: 617-452-4174; Fax: 617-452-3293; Email: djirvine@mit.edu)

Supplemental Methods on Chemokine Gradient Modeling

Governing equations

We modeled the secretion and transport of chemokine from isolated source cells, arrays of cells, or synthetic CRM beads using analytical solutions or COMSOL finite element modeling software to solve the equations for coupled reaction/diffusion appropriate to the physical system. The secreting cell was modeled as a sphere with diameter 20 μm located in an infinite space or in the center of a cubic space; CRMs were modeled as 30 μm-diameter spheres in line with the experimental bead size. Chemokine secretion from cells was modeled as production of chemokine at a constant rate at the surface of the cell.

In order to simulate the gradient fields developing around individual microspheres in our chemotaxis assays, we calculated the apparent diffusion constant for chemokine within individual alginate microspheres as previously described.[1] This effective diffusivity, D_{eff}, was determined by fitting experimentally-measured chemokine release from a suspension of microspheres over time at 37°C using a solution for Fick's Second Law applied to spherical geometry in sink conditions valid for time-points when < 40% of the total release has occurred[2]:

$$\frac{M_t}{M_\infty} = \sum_i w_i \left(6\left(\frac{D_{eff} t}{\pi R_i^2} \right)^{\frac{1}{2}} - \frac{3 D_{eff} t}{R_i^2} \right)$$

where M_t is the amount of chemokine release at time t, M_∞ is the total amount released at infinite time (i.e. total amount loaded in the particles), and w_i is the weight fraction of microspheres with radius R_i, summed over the distribution of all microsphere sizes. This

analysis accounted for the polydispersity of the microspheres and the sum over all particle sizes was carried out using the experimentally determined size distribution of the particles. Data was fit using the built-in nonlinear regression algorithm of Prism 5.0 software (GraphPad Software). Via ELISA measurements, there was no detectable binding of CCL19 or CCL21 to type I collagen (consistent with prior reports[3]) and no significant chemokine degradation over 12 hrs in collagen with 10% serum (data not shown). Therefore, for calculations of *in vitro* gradients generated in the ECM gels by CRMs, we assumed no matrix binding or attractant degradation.

The transport of the chemokines from the cell/bead surface to the surroundings was modeled as diffusion without convective flow, giving for the concentration change with time:

$$\frac{\partial C}{\partial t} = D\nabla^2 C - R_p - R_M$$

where C is the concentration of the attractant, D is the diffusion constant of chemokine in the tissue matrix, R_p is a reaction term for chemokine proteolysis/degradation, and R_M is a reaction term for chemokine binding to matrix (see Supplementary Table S1 for summary of model parameters). Following prior work,[4] because the porosity of the tissue matrix is on length scales much greater than the size of the chemokine, D was taken as half the diffusivity of chemokine in water, D_o. D_o was estimated using the empirical relationship:[5,6]

$$D_0 = \frac{A}{MW^{1/3}}$$

where A is a constant, 2.82×10^{-5} cm^2/s (g/mol)$^{1/3}$, and MW is the protein molecular weight. These relationships gave D_{CCL21} = 6.5x10^{-7} cm^2/s and D_{CCL19} = 7.21x10^{-7} cm^2/s. The reaction term R_p accounts for the chemokine proteolysis and other modes of clearance (such as consumption by non-relevant cells or lymphatic drainage) by a lumped first-order reaction. The reaction term R_M accounts for chemokine binding to or being released from the matrix, and values of this reaction rate were chosen specifically for CCL21 binding to heparan sulfate as done by Shields *et al*.[7]

Chemokine Decay

Modulation of chemokine activity by proteases provides a critical layer of regulation during cCRMades of host defense to enable rapid enzymatic modulation of chemokines. Chemokine decay by proteases can be described by Michaelis kinetics as following:

$$R_p = \frac{k_{cat} E_0 S}{K_m + S}$$

where S denotes the substrate concentration, which is the chemokine concentration C here, and k_{cat} is the catalytic rate constant and K_m is the Michaelis equilibrium constant. The substrate concentration S discussed here is small compared to K_m, so we can simplify the solution as:

$$R_p = \frac{k_{cat} E_0}{K_m} C = k_p C$$

where $k_p = k_{cat} E_0 / K_m$. To simplify calculations, we considered all modes of attractant clearance using this lumped first order clearance term.

The degradation of chemokines and growth factors by proteases has been extensively studied in the literature.[8] Degradation of a series of chemokines including CXCL12, CXCL10, CCL5, etc., by CD26/dipepetidyl peptidase IV have been extensively studied in Lambeir's work,[9] and showed striking selectivity with the chemokine family; a more detailed review of chemokine modification on carboxyl-terminal proteolysis or amino-terminal proteolysis was discussed in Zabel et al.[10] In the study of chemokine proteolysis by CD26, the k_{cat} ranges from 0.0026/s to 12/s and K_m varies around 1-25 μM. In normal human plasma, the enzyme CD26/DDP IV (~175 kDa) is present with a bioactivity of 25 U/L with a specific activity of 22 U/mg, which is equivalent to 5.7 nM of active enzyme.[11] Therefore, we estimated k_p based on the kinetics measured for other chemokines in this paper and made calculations with k_p = 0.0002/s, 0.001/s or 0.005/s to study the effect of degradation rate on the creation of gradients around a single cell. As a point of reference, the degradation rate for other growth factors, such as bFGF was measured as ~ 10^{-6}/s [8] and VGEF was estimated to be 10^{-4}-10^{-2}/s.[12] In Fleury and Swartz's study,[13] k_p was chosen as 0.2/s to examine the effects of proteolysis rates at the same order of magnitude as transport.

Chemokine Binding to Matrix

As highly basic small proteins, chemokines have the potential to bind to ECM proteins or be captured by GAGs on other cell surfaces. Many chemokines have been shown to bind to proteoglycans, which carry acidic sulfate carboxyl groups, especially heparan sulfate (HS) and its analogs.[14-16] CCL21 binding equilibrium to heparan sulfate on proteoglycans in matrigel was experimentally measured and used to predict CCL21 pericellular concentrations with

mathematical simulation in Shields et al.[7] We considered the interaction between CCL21 and the surrounding matrix using the reaction term:

$$R_M = k_f CM - k_r C_b$$

where M is the concentration of chemokine binding sites in the matrix and C_b is the concentration of chemokine bound to matrix, k_f was 9.3×10^4 $M^{-1}s^{-1}$ and k_r was 1.2×10^{-4} s^{-1}, measured in Shields et al.[7] In our calculations, we determined the effects of matrix binding by varying the concentration of matrix binding sites from 1.2 nM to 1.2 μM. For CCL19, it was assumed that there is no interaction with matrix, based on published analyses of CCL19 binding to GAGs[17-20] and our own experimental measurements.

Receptor desensitization and recycling

After receptor is ligated with a chemokine ligand, it can trigger downstream signaling but also be desensitized and internalized in a phosphorylation-dependent or -independent manner.[21,22] We employed a simple model for receptor internalization and desensitization to analyze the binding of CCL19 and CCL21 to CCR7, illustrated schematically here as

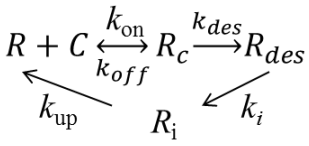

This simple receptor desensitization, internalization and recycling model was modified from Butcher and Lin's work modeling binding of chemokines to CCR7.[23] Here, R is the number of free receptors on the cell surface, R_c is the number of chemokine-complexed receptors, R_{des} is the number of desensitized receptors on the cell surface and R_i is the number of internalized receptors. Correspondingly, k_{on} is the binding rate of chemokine to receptor, k_{off} is dissociation rate of chemokine from receptor, k_{des} is the desensitization rate, k_i is the internalization rate and k_{up} is the rate of upregulation of receptor to the cell surface. This reaction scheme was described using a series of kinetic equations:

$$\frac{dR_c}{dt} = k_{on}RC - k_{off}R_c - k_{des}R_c$$

$$\frac{dR}{dt} = -k_{on}RC + k_{off}R_c + k_{up}R_i$$

$$\frac{dR_{des}}{dt} = k_{des}R_c - k_i R_{des}$$

$$R_T^0 = R + R_c + R_{des} + R_i$$

It is assumed that these reactions reach steady state and thus the active receptor ligated with chemokine was expressed as a function of these kinetic rate constants and total initial surface receptor number,

$$\frac{R_c}{R_T^0} = \left(1 + \frac{k_{off} + k_{des}}{k_{on}C} + \frac{k_{des}}{k_i} + \frac{k_{des}}{k_{up}}\right)^{-1}$$

Here, $K_d = \frac{k_{off}}{k_{on}}$ is the dissociation constant of chemokine-receptor binding. Likewise, we also define constants $K_{on}^{des} = \frac{k_{des}}{k_{on}}$, $K_i^{des} = \frac{k_{des}}{k_i}$ and $K_{up}^{des} = \frac{k_{des}}{k_{up}}$ for convenience. CCL19 and CCL21 bind to CCR7 with comparable affinities (both with estimated K_Ds of a few nM[24-26] and thus we chose $K_d^{CCL21} = K_d^{CCL19} = 5$ nM. However, unlike CCL21, CCL19 triggers rapid internalization of CCR7 and desensitization of CCR7 signaling.[27-29] In order to determine the kinetic parameters, K_{on}^{des}, K_i^{des} and K_{up}^{des}, we fitted experimental measurements of the surface receptor expression following stimulation with various CCL19 concentrations (Fig. S2) to the predicted analytical solution at steady state:

$$\frac{R_T}{R_T^0} = \frac{R + R_c + R_{des}}{R_T^0} = \frac{1 + \frac{K_{on}^{des} + K_d}{C} + K_i^{des}}{1 + \frac{K_{on}^{des} + K_d}{C} + K_i^{des} + K_{up}^{des}}$$

Best-fit parameters were K_{on}^{des} = 3 nM, K_i^{des} = 8 nM, and K_{up}^{des} = 6 nM.

Modeling dense fields of chemokine sources

In the isolated chemokine source model, a single chemokine-secreting cell or chemokine-releasing bead was placed in the center of an infinite space. To model secreting cells/CRMs present at a finite density in tissue, we also conducted simulations of concentration gradients developed around individual beads/cells located in a field of sources uniformly distributed on a square lattice in space with various densities. The dimension of the cubic space, *a*, in which individual cells were located, i.e., the spacing between neighboring cells, was varied from 50 μm to 500 μm.

Boundary conditions and solutions

The model is based on the assumption that the cells are perfectly round with radius ρ = 10 μm and are secreting chemokines symmetrically from their surface at constant rate, *Q*, 0.01-1 pg/hr/cell covering the physiologic ranges estimated for lymphatic endothelial cells and mature dendritic cells.[30-33] Single secreting cells were modeled in the center of an infinite space as in [34] while individual secreting cells surrounded by other secreting cells in a tissue were modeled as occupying the center of a defined cubic space, with dimensions equal to the distance between secreting cells, with boundary conditions set to zero chemokine flux. The solution to the governing equation considering chemokine degradation only in infinite space has an analytical solution for the steady state:

$$C = \frac{Qexp\left(-\sqrt{\frac{k_p}{D}}r\right)}{4\pi Dr\left(\sqrt{\frac{k_p}{D}}\rho + 1\right)exp\left(-\sqrt{\frac{k_p}{D}}\rho\right)}$$

The transient solution for the above system and the steady state solution to the governing equation considering both chemokine degradation and matrix binding with defined space dimensions were solved using the *transport of dilute species* module in COMSOL modeling software (COMSOL Inc., Burlington, MA). Solutions of the diffusion equations were solved for free triangular FEM mesh points of maximum spacing, 8 μm and minimum spacing, 16 nm.

Receptor occupancy gradient ΔR_c

The difference in actual occupied receptor number between the front and back of responding cells (which we will also refer to as the receptor occupancy gradient, ΔR_c), was calculated from the equations governing receptor-ligand binding accounting for the concentration gradients of attractant. For non-desensitized receptors after ligand stimulation, the receptor occupancy gradient was calculated as:

$$\Delta R_c = R_T \frac{(C + K_d)}{C^2(1 + \frac{K_d}{C})^2}\frac{dC}{dr}\Delta r$$

where Δr is the length of the responding cell from front to rear. For desensitizing receptors, the Lin/Butcher model as described above was used to capture desensitization, internalization, and recycling processes. In this case, the receptor occupancy gradient was defined as:

$$\Delta R_c = R_T^0 \frac{(C + K_{on}^{des} + K_d)}{C^2(1 + \frac{K_{on}^{des} + K_d}{C} + K_i^{des} + K_{up}^{des})^2} \frac{dC}{dr} \Delta r$$

Supplementary Methods References

1 Wang, Y. & Irvine, D. J. Engineering chemoattractant gradients using chemokine-releasing polysaccharide microspheres. *Biomaterials* **32**, 4903-4913, doi:10.1016/j.biomaterials.2011.03.027 (2011).

2 Crank, J. *The Mathematics of Diffusion*. (Clarendon Press, 1975).

3 Haessler, U., Pisano, M., Wu, M. & Swartz, M. A. Dendritic cell chemotaxis in 3D under defined chemokine gradients reveals differential response to ligands CCL21 and CCL19. *Proc Natl Acad Sci U S A* **108**, 5614-5619, doi:1014920108 [pii]
10.1073/pnas.1014920108 (2011).

4 Zhao, X., Jain, S., Benjamin Larman, H., Gonzalez, S. & Irvine, D. J. Directed cell migration via chemoattractants released from degradable microspheres. *Biomaterials* **26**, 5048-5063 (2005).

5 Lauffenburger, D. A., Tranquillo, R. T. & Zigmond, S. H. Concentration gradients of chemotactic factors in chemotaxis assays. *Methods Enzymol* **162**, 85-101 (1988).

6 Tanford, C. *Physcial Chemistry of Macromolecules*. (Wiley, 1961).

7 Shields, J. D. *et al.* Autologous chemotaxis as a mechanism of tumor cell homing to lymphatics via interstitial flow and autocrine CCR7 signaling. *Cancer Cell* **11**, 526-538, doi:S1535-6108(07)00145-6 [pii]
10.1016/j.ccr.2007.04.020 (2007).

8 Tong, S. & Yuan, F. Numerical simulations of angiogenesis in the cornea. *Microvasc Res* **61**, 14-27, doi:10.1006/mvre.2000.2282
S0026-2862(00)92282-9 [pii] (2001).

9 Lambeir, A. M. *et al.* Kinetic investigation of chemokine truncation by CD26/dipeptidyl peptidase IV reveals a striking selectivity within the chemokine family. *J Biol Chem* **276**, 29839-29845, doi:10.1074/jbc.M103106200
M103106200 [pii] (2001).

10 Zabel, B. A. *et al.* Chemoattractants, extracellular proteases, and the integrated host defense response. *Exp Hematol* **34**, 1021-1032, doi:S0301-472X(06)00314-6 [pii]
10.1016/j.exphem.2006.05.003 (2006).

11 Proost, P. *et al.* Cleavage by CD26/dipeptidyl peptidase IV converts the chemokine LD78beta into a most efficient monocyte attractant and CCR1 agonist. *Blood* **96**, 1674-1680 (2000).

12 Vempati, P., Mac Gabhann, F. & Popel, A. S. Quantifying the proteolytic release of extracellular matrix-sequestered VEGF with a computational model. *PLoS One* **5**, e11860, doi:10.1371/journal.pone.0011860 (2010).

13 Fleury, M. E., Boardman, K. C. & Swartz, M. A. Autologous morphogen gradients by subtle interstitial flow and matrix interactions. *Biophys J* **91**, 113-121, doi:S0006-3495(06)71712-X [pii]
10.1529/biophysj.105.080192 (2006).

14 Proudfoot, A. E. *et al.* Glycosaminoglycan binding and oligomerization are essential for the in vivo activity of certain chemokines. *Proc Natl Acad Sci U S A* **100**, 1885-1890 (2003).

15 Wagner, L. *et al.* Beta-chemokines are released from HIV-1-specific cytolytic T-cell granules complexed to proteoglycans. *Nature* **391**, 908-911 (1998).

16 Ali, S. *et al.* A non-glycosaminoglycan-binding variant of CC chemokine ligand 7 (monocyte chemoattractant protein-3) antagonizes chemokine-mediated inflammation. *J Immunol* **175**, 1257-1266 (2005).

17 Hirose, J., Kawashima, H., Yoshie, O., Tashiro, K. & Miyasaka, M. Versican interacts with chemokines and modulates cellular responses. *J Biol Chem* **276**, 5228-5234 (2001).

18 Patel, D. D. *et al.* Chemokines have diverse abilities to form solid phase gradients. *Clin Immunol* **99**, 43-52 (2001).

19 Uchimura, K. *et al.* HSulf-2, an extracellular endoglucosamine-6-sulfatase, selectively mobilizes heparin-bound growth factors and chemokines: effects on VEGF, FGF-1, and SDF-1. *BMC Biochem* **7**, 2, doi:1471-2091-7-2 [pii]
10.1186/1471-2091-7-2 (2006).
20 Yang, B. G. *et al.* Binding of lymphoid chemokines to collagen IV that accumulates in the basal lamina of high endothelial venules: its implications in lymphocyte trafficking. *J Immunol* **179**, 4376-4382, doi:179/7/4376 [pii] (2007).
21 DeFea, K. A. Stop that cell! Beta-arrestin-dependent chemotaxis: a tale of localized actin assembly and receptor desensitization. *Annu Rev Physiol* **69**, 535-560, doi:10.1146/annurev.physiol.69.022405.154804 (2007).
22 Devreotes, P. N. & Zigmond, S. H. Chemotaxis in eukaryotic cells: a focus on leukocytes and Dictyostelium. *Annu Rev Cell Biol* **4**, 649-686, doi:10.1146/annurev.cb.04.110188.003245 (1988).
23 Lin, F. & Butcher, E. C. Modeling the role of homologous receptor desensitization in cell gradient sensing. *J Immunol* **181**, 8335-8343, doi:181/12/8335 [pii] (2008).
24 Willimann, K. *et al.* The chemokine SLC is expressed in T cell areas of lymph nodes and mucosal lymphoid tissues and attracts activated T cells via CCR7. *Eur J Immunol* **28**, 2025-2034 (1998).
25 Yoshida, R. *et al.* Secondary lymphoid-tissue chemokine is a functional ligand for the CC chemokine receptor CCR7. *J Biol Chem* **273**, 7118-7122 (1998).
26 Ott, T. R. *et al.* Determinants of high-affinity binding and receptor activation in the N-terminus of CCL-19 (MIP-3 beta). *Biochemistry* **43**, 3670-3678 (2004).
27 Bardi, G., Lipp, M., Baggiolini, M. & Loetscher, P. The T cell chemokine receptor CCR7 is internalized on stimulation with ELC, but not with SLC. *Eur J Immunol* **31**, 3291-3297, doi:10.1002/1521-4141(200111)31:11<3291::AID-IMMU3291>3.0.CO;2-Z [pii]
10.1002/1521-4141(200111)31:11<3291::AID-IMMU3291>3.0.CO;2-Z (2001).
28 Byers, M. A. *et al.* Arrestin 3 mediates endocytosis of CCR7 following ligation of CCL19 but not CCL21. *J Immunol* **181**, 4723-4732, doi:181/7/4723 [pii] (2008).
29 Kohout, T. A. *et al.* Differential desensitization, receptor phosphorylation, beta-arrestin recruitment, and ERK1/2 activation by the two endogenous ligands for the CC chemokine receptor 7. *J Biol Chem* **279**, 23214-23222 (2004).
30 Chieppa, M. *et al.* Cross-linking of the mannose receptor on monocyte-derived dendritic cells activates an anti-inflammatory immunosuppressive program. *J Immunol* **171**, 4552-4560 (2003).
31 Lebre, M. C. *et al.* Differential expression of inflammatory chemokines by Th1- and Th2-cell promoting dendritic cells: a role for different mature dendritic cell populations in attracting appropriate effector cells to peripheral sites of inflammation. *Immunol Cell Biol* **83**, 525-535, doi:ICB1365 [pii]
10.1111/j.1440-1711.2005.01365.x (2005).
32 Sallusto, F. *et al.* Distinct patterns and kinetics of chemokine production regulate dendritic cell function. *Eur J Immunol* **29**, 1617-1625, doi:10.1002/(SICI)1521-4141(199905)29:05<1617::AID-IMMU1617>3.0.CO;2-3 [pii]
10.1002/(SICI)1521-4141(199905)29:05<1617::AID-IMMU1617>3.0.CO;2-3 (1999).
33 Issa, A., Le, T. X., Shoushtari, A. N., Shields, J. D. & Swartz, M. A. Vascular endothelial growth factor-C and C-C chemokine receptor 7 in tumor cell-lymphatic cross-talk promote invasive phenotype. *Cancer Res* **69**, 349-357, doi:10.1158/0008-5472.CAN-08-1875 (2009).
34 Francis, K. & Palsson, B. O. Effective intercellular communication distances are determined by the relative time constants for cyto/chemokine secretion and diffusion. *Proc Natl Acad Sci U S A* **94**, 12258-12262 (1997).

35 Stachowiak, A. N., Wang, Y., Huang, Y. C. & Irvine, D. J. Homeostatic lymphoid chemokines synergize with adhesion ligands to trigger T and B lymphocyte chemokinesis. *J Immunol* **177**, 2340-2348, doi:177/4/2340 [pii] (2006).

Table S1. Summary of model parameters

Category	Parameter	Value†				Suppl. Methods references
Basic	Radius of chemokine secreting cell, ρ (μm)	**10**				–
	Radius of receiving cell, ω (μm)	**5**				–
	Secretion rate (pg/hr/cell)	**1**	0.1	0.01		[30-33]
	Diffusion constant (cm^2/s)	CCL21	CCL19	CXCL12	CXCL10	
		6.5×10^{-7}	**7.21×10^{-7}**	**7.45×10^{-7}**	**7.24×10^{-7}**	[5,6]
	Space dimension, *a* (μm)	50	100	200	**500**	
Degradation	Rate constant (s^{-1})	0.005	**0.001**	0.0002		[8-13]
CCL21 binding to matrix	forward rate constant, k_f ($M^{-1}s^{-1}$)	**9.3×10^{4}**				[7]
	Backward rate constant, k_r (s^{-1})	**1.2×10^{-4}**				[7]
	Binding equilibrium constant, K_M (nM)	**1.29**				[7]
	Binding site concentration, *M* (μM)	**1.2**	0.12	0.012		[14-16]
	K_M/ *M*	**1000**	100	10		
Receptor binding and desensitization		CCL21	CCL19	CXCL12	CXCL10	
	Affinity, K_d (nM)	**5**	**5**	**3.0**	**2.5**	[24-26]
	Desensitization constant, K_{on}^{des} (nM)	**0**	**3**	**NA**	**1**	measured (Fig. S2)
	Internalization constant, K_i^{des}(nM)	**0**	**6**	**NA**	**0.2**	measured (Fig. S2)
	Upregulation constant, K_{up}^{des} (nM)	**0**	**8**	**NA**	**1**	measured (Fig. S2)

† default values used in the modeling shown in bold

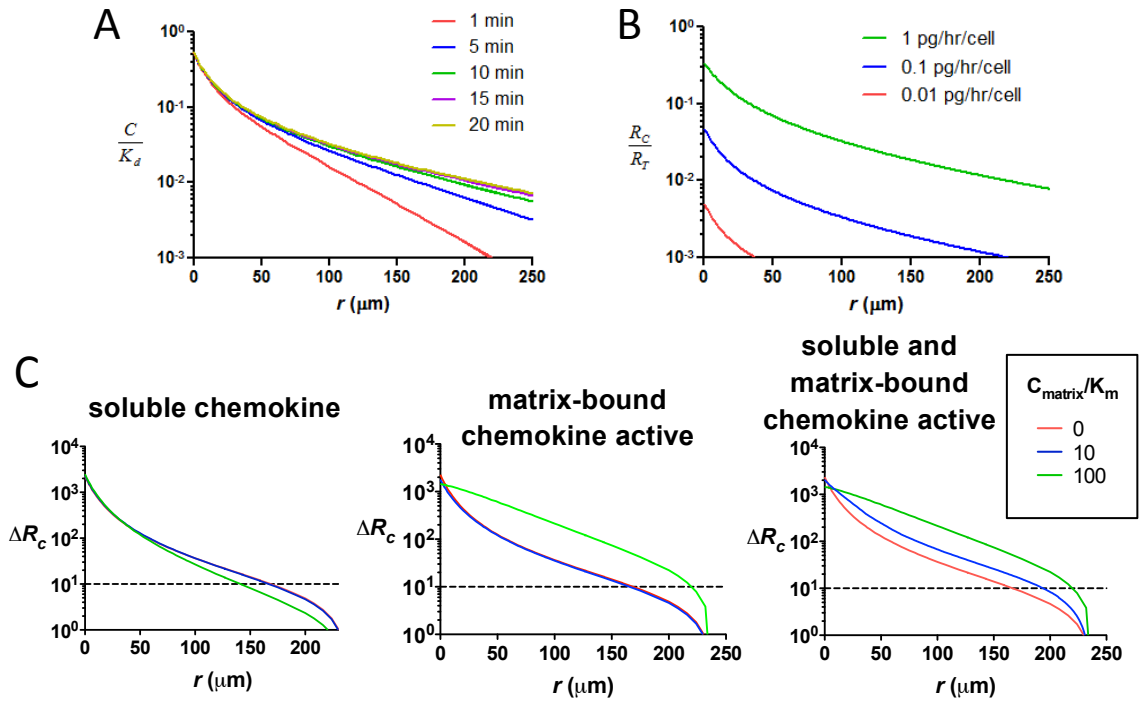

Figure S1. Chemokine gradients developing around isolated secreting cells. (A) Temporal evolution of CCL21 concentration profile calculated for a secretion rate of $1x10^{-4}$ ng/hr/cell. (B) Steady-state fraction of occupied receptors around an individual secreting cell at position $r = 0$ were calculated for different attractant secretion rates covering the physiologically relevant range. (C) Impact of matrix binding on steady state responding cell CCR7 receptor occupancy difference ΔR_c: FEM calculations were made for secreting cells 20 μm in diameter at the center of an infinite space secreting CCL21 at a constant rate of 1 pg/hr•cell. Shown are attractant concentration and receptor occupancy gradient profiles as a function of distance from the surface of the secreting cell. C_{matrix}/K_M is the ratio of the concentration of chemokine binding sites to the chemokine-matrix binding affinity ($k_r = 1.2x10^{-4}$/s and $k_f = 93$ mol/m^3/s). Shown are profiles generated assuming that only free chemokine binds receptors, only matrix-bound attractant binds receptors, or both soluble and matrix-bound attractant is active.

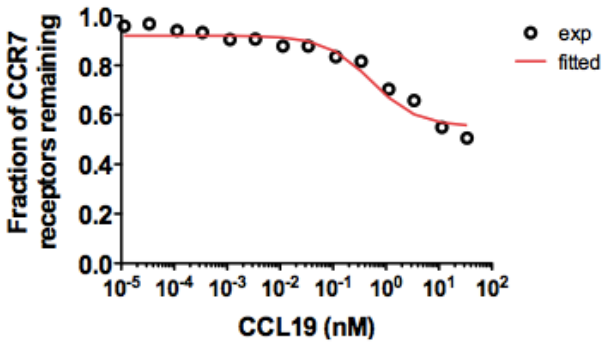

Figure S2. CCR7 internalization after CCL19 stimulation. Flow cytometry was used to measure CCR7 surface expression on resting human T-cells after incubation with CCL19 at the

indicated concentrations for 0.5 hr at 37°C, followed by washing with cold medium 3X and staining with APC-CCR7 Ab (3D12, Ebioscience). Shown are mean ± SEM as open circles; solid line is best fit to the CCL19/CCR7 receptor desensitization model (K_D = 5 nM, k_{des}/k_{on} = 3nM, k_{des}/k_{in} =6 nM, k_{des}/k_{up} = 8 nM).

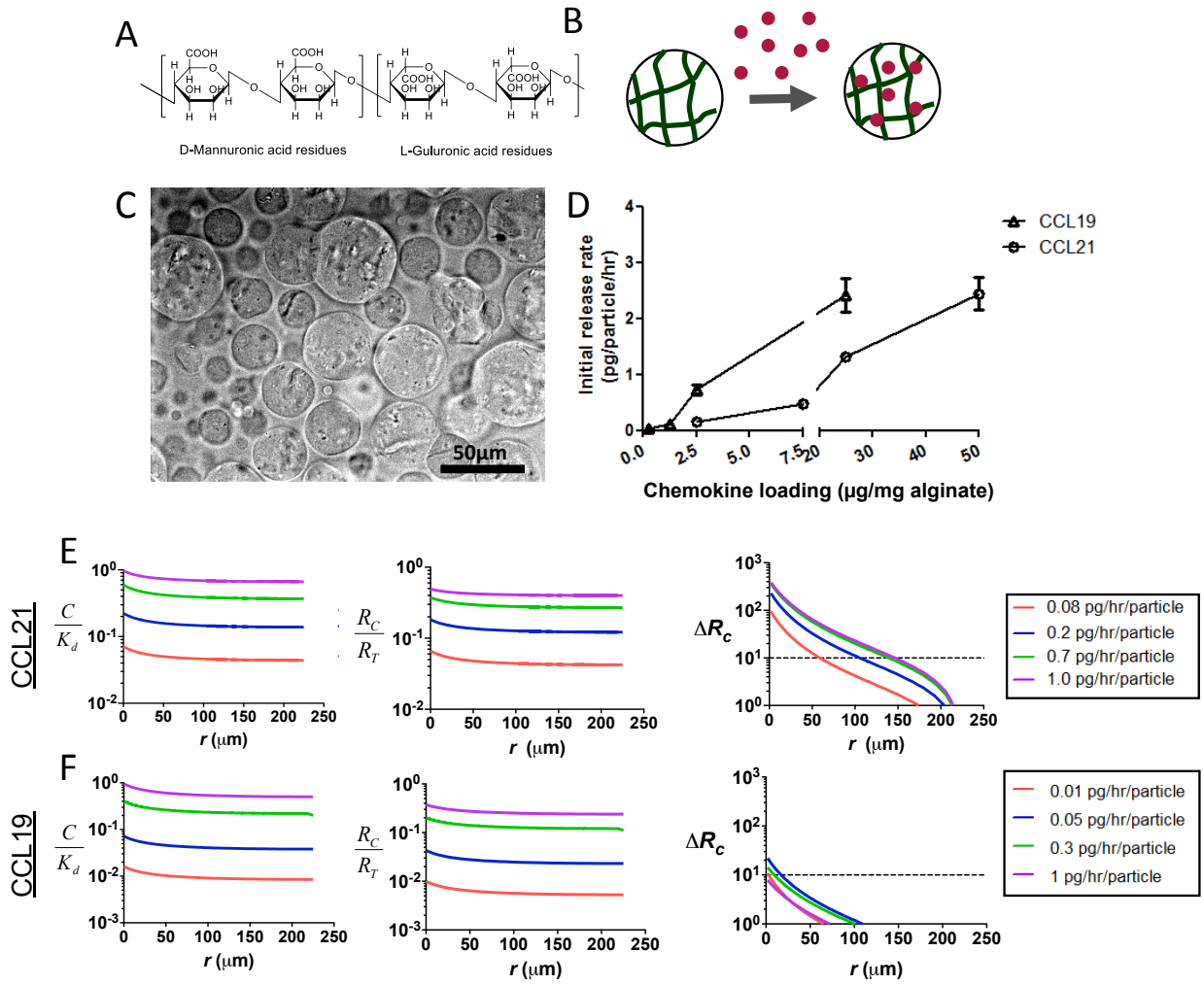

Figure S3. Synthesis and gradient generation with attractant-loaded alginate Chemokine-Releasing Microspheres. (A) Chemical structure of alginate. (B) Schematic of chemokine loading into alginate beads via post-bead-synthesis adsorption. (C) Bright field micrograph of alginate CRMs. (D) Initial release rate of CCL19 or CCL21 from alginate CRMs (over first 0.5 hr) as a function of attractant loading. (E, F) Modeling of gradient generation around isolated microspheres: Calculated attractant concentration profiles, fraction of receptors engaged, and ΔR_c for responding T-cells as a function of the distance to an isolated CRM at t = 30 min, determined for 30 μm diam. beads releasing CCL21 (E) or CCL19 (F) at the indicated initial release rates. Dashed lines on ΔR_c plots mark the theoretical threshold for stimulating migration.

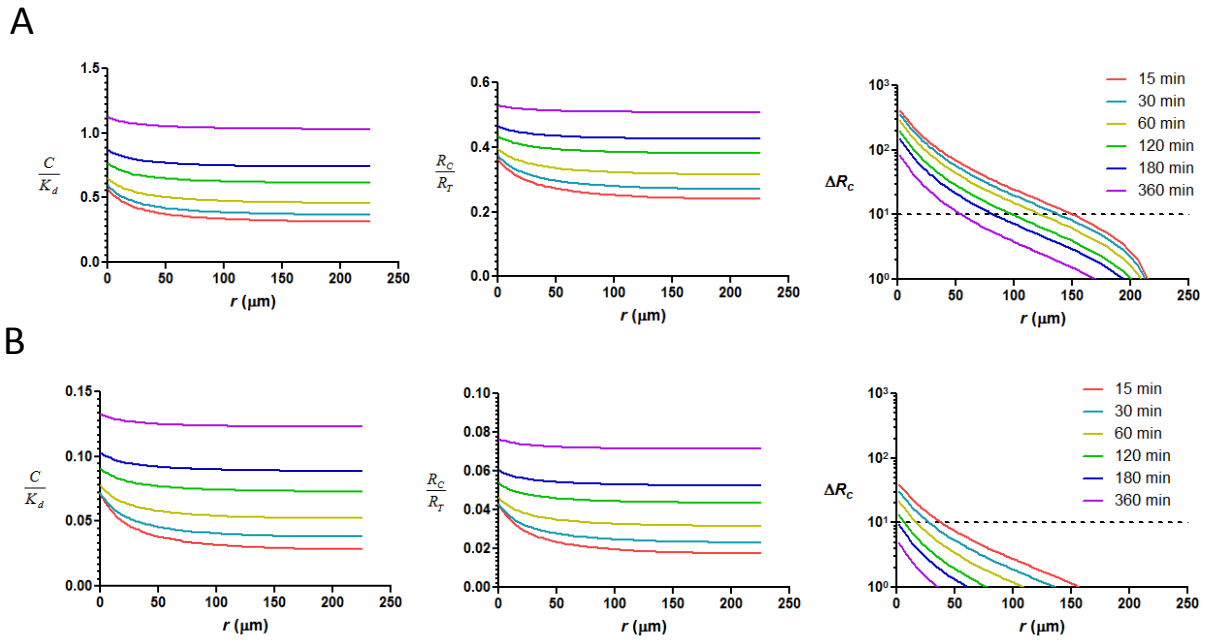

Figure S4. Time evolution of concentration and receptor occupancy profiles for T-cells responding to chemokine-releasing CRMs in collagen *in vitro*. Calculated attractant concentration profiles, fraction of occupied chemokine receptors (R_c/R_T), and receptor occupancy gradients (ΔR_c) over time for CRMs releasing CCL21 (A) or CCL19 (B) at experimentally-measured initial release rates of 6.7×10^{-4} ng/hr/particle (7.5 μg CCL21 loaded per mg alginate) and 5.2×10^{-5} ng/hr/particle (1 μg CCL19 loaded per mg alginate), respectively.

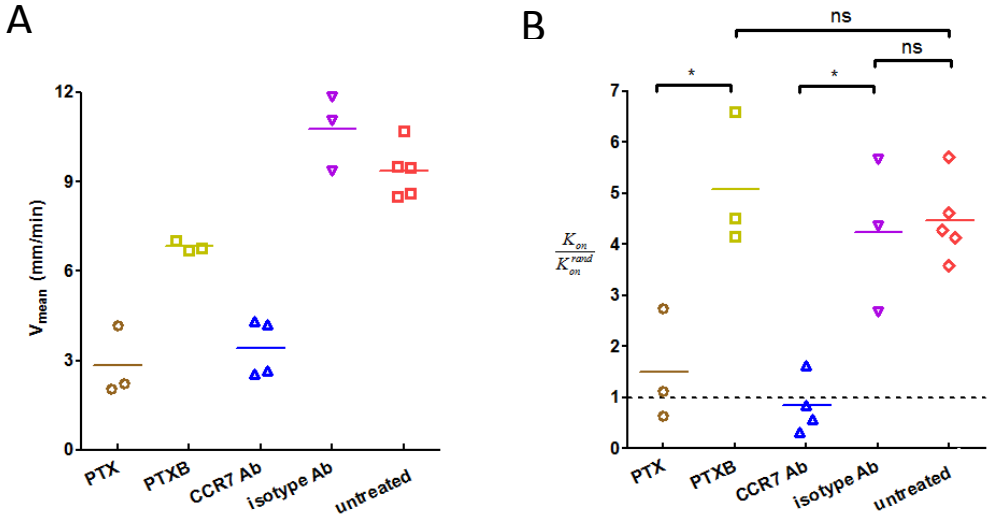

Figure S5. Increased encounter frequency with CCL21-CRM is CCL21 dependent. Resting human T-cells were treated with pertussis toxin (PTX) or its inactive B subunit as a control (PTXB) as previously described,[35] then embedded in collagen gels and imaged for 30 min in the presence of CCL21-releasing CRMs (initial release rate of 6.7×10^{-4} ng/hr/bead) to measure their velocity and bead hit rate. In parallel, a second set of T-cells were blocked with 10 μg/mL anti-

CCR7 (or isotype control antibody) for 30 min at 4°C, then introduced into collagen with CRMs in the presence of 10 µg/mL blocking or control antibody and imaged for 30 min. Shown are mean velocities (A) and hit rate ratios (B) determined from 30 min of videomicroscopy.

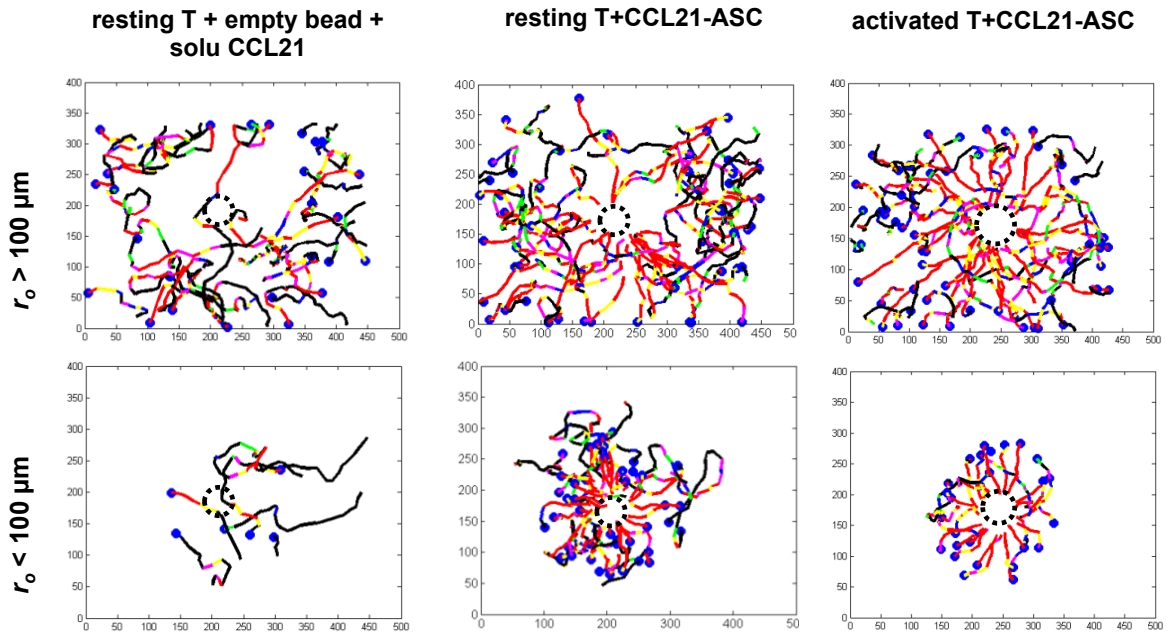

Figure S6. Migration paths of T-cells chemotaxing toward CCL21-releasing CRMs. Resting or activated human T-cells were embedded in collagen gels and imaged by videomicroscopy for 1.5 hr as in Fig. 4. In parallel, control samples of T-cells and empty CRMs in collagen mixed with 10 µg/mL "free" CCL21 were imaged. Shown are single-cell paths for cells whose starting positions (r_o) were greater than or less than 100 µm from the nearest bead, color-coded by the ICI value of the cell at each time interval (red ICI>0.8; yellow: 0.8>ICI>0.6; magenta: 0.6>ICI>0.4; blue: 0.4>ICI>0.2; green: 0.2>ICI>0; black: ICI<0).

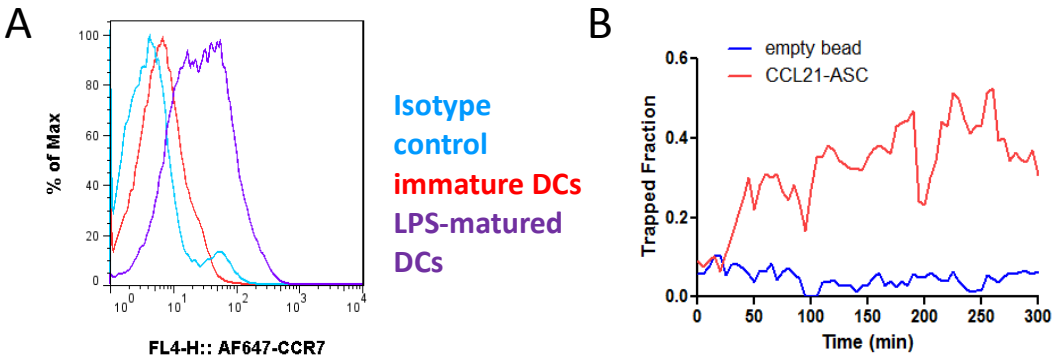

Figure S7. Activated human T-cells and mature dendritic cells persistently swarming around CCL21-CRM. (A) CCR7 expression on immature vs. LPS-treated mature monocyte-derived dendritic cells. (B) Trapped fraction evolution (0–5 h) of mature dendritic cells around CRMs releasing CCL21 at 0.7 pg/hr/particle vs. DCs migrating near empty beads.

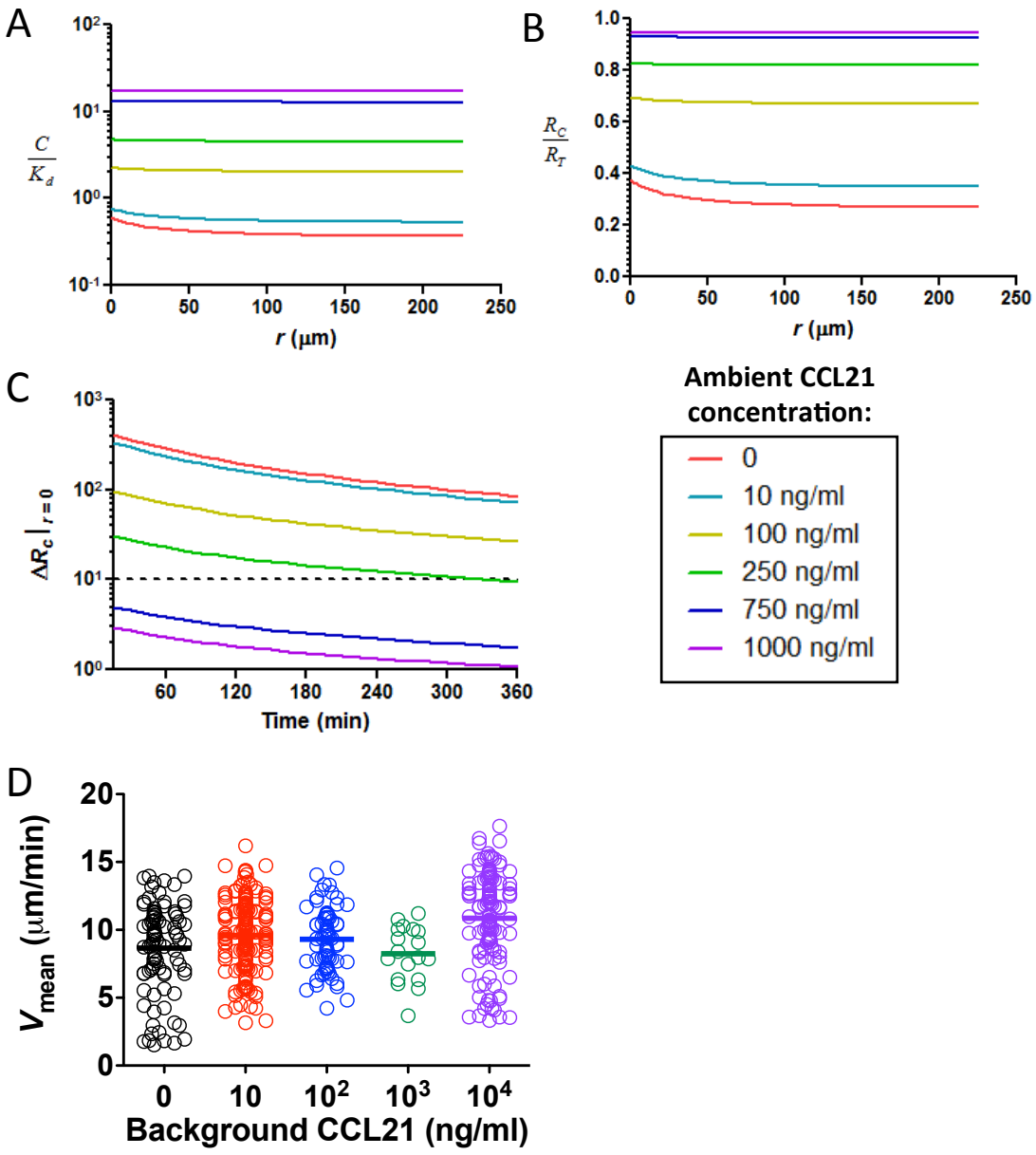

Figure S8. Decay of receptor occupancy gradient in responding T-cells as a function of time around individual CCL21-CRMs in the presence of increasing "background" free CCL21 in the matrix. (A-C) CCL21 concentration profiles were calculated for CCL21-CRMs ($(8x10^3$ beads/cm^3, 7.5 μg CCL21 loaded per mg alginate) with surrounding ambient CCL21 concentrations varying from 10 ng/ml to 1 μg/ml as indicated. Shown are calculated normalized CCL21 concentration (A) and fraction of occupied receptors (B) as a function of distance from the bead surface at t = 30 min. (C) CCR7 receptor occupancy gradients in individual T-cells at the point of contact with a CCL21-releasing bead are shown over time for different ambient CCL21 concentrations present in the matrix. (D) Experimental mean velocities of cells for different background levels of ambient chemokine in the matrix.

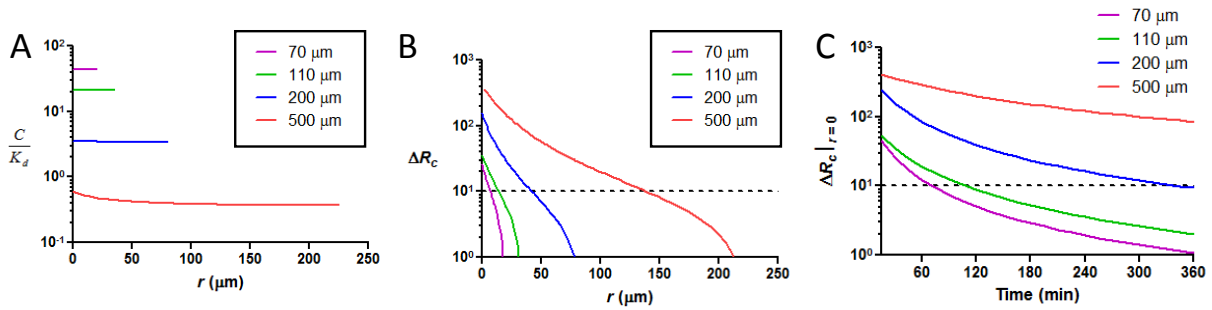

Figure S9. Modeling predicts attraction near individual beads in dense-bead source setting. (A-C) CCL21 concentration profiles and resulting receptor occupancy differences were calculated around individual CCL21-CRMs (7.5 µg CCL21 loaded per mg alginate) present at varying densities in regular 3D arrays (as in Fig. 2A), with bead center-to-center separations as indicated. Shown are normalized CCL21 concentration (A) and receptor occupancy gradients (B) as a function of distance from the bead surface at 30 min, and ΔR_c at the bead surface as a function of time (C).

Video S1. Random migration of resting human T-cells around empty CRMs in the presence of 10 μg/ml soluble CCL21. Resting human T-cells labeled with CMTPX (red) were mixed with empty FITC-labeled alginate beads at the density of $8x10^3$ particles/cm^3 and imaged in time-lapse. Top panel: brightfield; Bottom panel: fluorescence overlay; scale bar 50 μm; time stamp is in min:sec.

Video S2. Attraction of resting human T-cells to CCL21-CRMs. Alginate CRMs releasing CCL21 at a rate of $6.7x10^{-4}$ ng/hr/particle at a density of $8x10^3$ particles/cm^3 were suspended with resting human T-cells (CMTPX-labeled, red) in collagen and imaged in time-lapse. Shown is a field of view from time zero around one isolated CRM (labeled by incorporation of 1% Alexafluor-488-labeled CCL21). Top panel: brightfield; bottom panel fluorescence overlay; scale bar 50 μm; time stamp is in min:sec.

Video S3. Persistent swarming of resting human T-cells induced by CCL21-CRMs. CCL21-CRMs releasing CCL21 at a rate of $6.7x10^{-4}$ ng/hr/particle at a density of $8x10^3$ particles/cm^3 were suspended with resting human T-cells in collagen and imaged in time-lapse. Shown is brightfield imaging, scale bar 50 μm; time stamp is in hr:min.

Video S4. CCL19-CRMs fail to induce stable chemoattraction of resting T-cells. CCL19-CRMs releasing CCL19 at a rate of $5.2x10^{-5}$ ng/hr/particle at a density of $8x10^3$ particles/cm^3 were suspended with resting human T-cells (CMTPX-labeled, red) in collagen and imaged by time-lapse microscopy. Shown is a field of view centered on an isolated CRM (dimly defined by phase contrast in brightfield). T-cells transiently accumulate on the bead surface but quickly migrate away. Top panel: bright field; Bottom panel: T-cell fluorescence image; scale bar 50 μm; time stamp is in min:sec.

Video S5. Attraction and persistent swarming of human mature dendritic cells around individual CCL21-CRMs. CCL21-CRMs releasing CCL21 at a rate of $6.7x10^{-4}$ ng/hr/particle at a density of $8x10^3$ particles/cm^3 were suspended in collagen with human dendritic cells and imaged in time-lapse. Shown is brightfield imaging centered on an isolated CRM over 6 hrs; scale bar 50 μm; time stamp is in hr:min:sec.

Video S6. Attraction and persistent swarming of human activated T-cells in the field of CCL21-CRMs at the spacing of 50 μm between beads. CCL21-CRMs releasing CCL21 at a rate of $6.7x10^{-4}$ ng/hr/particle were suspended in collagen with activated T-cells at a high bead density where the mean separation between beads was 100 μm. CCL21-CRMs were labeled green by inclusion of 1% Alexa fluor 488-CCL21 and activated T-cells were labeled with the red cytosolic dye, CMTPX. Top panel: brightfield, lower panel: fluorescence overlay; scale bar 50 μm; time stamp is in hr:min